Polymer 72 (2015) 10–20

Contents lists available at ScienceDirect

Polymer

journal homepage: www.elsevier.com/locate/polymer

Designing three-dimensional ordered structures from directed self-assembly of block copolymer films in topographical templates

Xuguang Cao, Liangshun Zhang*, Jiabin Gu, Liquan Wang, Jiaping Lin**

Shanghai Key Laboratory of Advanced Polymeric Materials, State Key Laboratory of Bioreactor Engineering, Key Laboratory for Ultrafine Materials of Ministry of Education, School of Materials Science and Engineering, East China University of Science and Technology, Shanghai 200237, China

ARTICLE INFO

Article history:
Received 28 April 2015
Received in revised form
15 June 2015
Accepted 5 July 2015
Available online 8 July 2015

Keywords:
Directed self-assembly
Block copolymers
Computer simulations

ABSTRACT

Directed self-assembly of block copolymers offers a novel paradigm for building up three-dimensional (3D) device-oriented nanostructures towards deep sub-100-nm resolution. To clearly unveil the 3D patterns with long-range order, we herein utilize computer simulations to explore the directed self-assembly behaviors of cylindrical-forming block copolymer films in topographical templates. Unlike the 3D architectures in the bulk, the cylinder orientations in various layers of 3D ordered structures are independently manipulated by modulating the design parameters of topographical templates. Moreover, a set of design strategies are proposed to precisely construct the 3D non-trivial structures with T-junctions and jogs at desired locations and layers. Importantly, the simulations clarify the experimental observations about the formation range of 3D interconnected structures, and manifest that the vertical interconnections depend strongly on the template thickness. These results provide detailed insights into the nature of 3D assembled structures, and furthermore offer promising strategies for constructing the 3D device-oriented elements such as T-junctions, jogs and interconnections.

1. Introduction

Three-dimensional (3D) structures with long-range order in small scales captivate the minds of scientists because they enable a number of key innovations for photonic crystals or metamaterials [1,2], organic photovoltaics [3,4], nanoelectronics [5–7] and so forth. But as the structure features are pushed towards deep sub-100-nm scales, conventional processes and traditional materials in electron-beam lithography and photolithography are hindered either by the inherent diffraction limits of light or by the expense of sophisticated facilities [8]. To circumvent these shortcomings, experimentalists have pursued numerous alternative or complementary technologies to precisely construct the ordered nanostructures via the directed assembly of soft materials, such as DNA, colloids and block copolymers [9–22]. Among these materials, the block copolymers are able to spontaneously self-assemble into a rich variety of 3D periodic structures including sphere, cylinders and lamellae with dimensions of ~10–50 nm [23,24].

Integrating the directed assembly methodology and the inherently 3D characteristics of block copolymer nanostructures offers a new paradigm for fabricating the 3D controllable nanostructures with long-range order in a single self-assembly step [25–30], which goes beyond the planar fabrication process of lithographic methods. A recent example of the integrated approach is provided by bilayer films of cylindrical-forming block copolymers in topographical templates [31]. It is demonstrated that the block copolymers are guided to self-assemble into the 3D ordered nanostructures consisting of the cylinders with controlled orientation. Furthermore, the integrated method opens a door to create 3D device-oriented elements towards deep sub-100-nm resolution such as cross-point-like architectures, T-junctions and interconnections, which are cumbersome to be fabricated in a single step via the soft-lithographic approaches [32,33].

Although the directed self-assembly of block copolymers offers the promising opportunity to build up the 3D ordered structures with controlled orientation, the microscopic details of such patterns remain to be definitely elucidated. One particular aspect of the problem concerns the orientation behavior of block copolymer domains in various layers. However, it is currently difficult to directly visualize the interior of 3D structures in experiments, although tremendous progresses have been made towards characterizing the complex architectures at nanometer scales [34,35].

* Corresponding author.
** Corresponding author.
E-mail addresses: zhangls@ecust.edu.cn (L. Zhang), jlin@ecust.edu.cn (J. Lin).

http://dx.doi.org/10.1016/j.polymer.2015.07.007
0032-3861/

One viable approach to promote a better understanding of the 3D structures is computer simulations, which allow us to inspect the unique features of 3D architectures in more details. Another hindrance to construct the architectures from the block copolymers is that design rules for the 3D device-oriented structures considerably lag the significant strides achieved in planar structures. Advanced design methodologies for the two-dimensional structures of block copolymer films are not sufficient to manage the added complexity caused by the third dimension [36–38]. Consequently, it is of interest to explore whether computer simulations could be utilized to rationally design the 3D device-oriented structures such as mesh-shaped architectures, controlled defects and interconnected superstructures, which foreshadow the potential to fabricate 3D integrated-circuit elements [39,40].

The directed self-assembly behaviors of block copolymer films have been examined by the theory and simulations [27,41–50]. For instance, Ramírez-Hernández et al. used the Monte Carlo simulations of a coarse-grained model to investigate the morphologies of lamella-forming block copolymers [27]. A series of novel 3D structures have been identified through the directed self-assembly between two chemically patterned surfaces. One drawback of these studies is that the simulations are performed in small cells containing the microstructures with one or two periodicities. Such calculations for the directed self-assembly of block copolymer films cannot capture the order behaviors of microstructures and predict the non-periodic structures with controlled defects, which are of crucial importance to the advancement of nanotechnology for precision and large-area nanofabrication.

To address the above challenges, we herein introduce a mesoscale computational model to explore the 3D self-assembled structures of block copolymer films in the large scales. Our model is based on the self-consistent field theory (SCFT) of polymeric fluids [51–56], which explicitly comprises the contribution of configuration entropy of polymer chains. The SCFT is essentially a coarse-grained model of polymer chains, allowing researchers to probe into the order behavior of domains and the non-periodic structures of block copolymers in large scale systems within computationally realistic time. Recently, we developed a parallel algorithm of SCFT to capture the orientation behavior of monolayer cylinders of block copolymers in the topographical templates [55]. It is confirmed that the long-range order of cylinders with single orientation is enhanced by virtue of the anisotropic posts, and the complex patterns with controlled defects are realized via rationally designing the layouts of post arrays.

In the present study, we extended the model of cylinder monolayer to describe the system of bilayers of cylinders with different orientations, and carried out the large cell simulations of SCFT to fully grasp the universal principles for building up the 3D superstructures of cylindrical-forming block copolymers in the topographical templates. The deformation degree of cylinders is analyzed as functions of the geometrical characteristics of posts and the periodicities of post lattice. To the best of our knowledge, the large cell simulations of SCFT constitute the first study about the deformation degree of block copolymer domains in various layers of 3D architectures. We then arrived at the design strategies for creating the 3D non-periodic structures with T-junctions at desired locations and layers, and presented the design rules for making the interconnections between the top and bottom layers. We closed with a comparison of the 3D ordered architectures with the novel patterns of bilayer block copolymer films in the experiments. The study provides a detailed example of SCFT simulations to evaluate and design the 3D complex patterns with a prospect of their further development for nanoelectronic applications.

2. Model

To explore the directed self-assembly behavior of cylindrical-forming block copolymers in the topographical templates, the model adopted here is based on the standard Hamiltonian used in the polymeric field-theoretic approach with the mean-field approximation. We consider a system with volume V, which consists of block copolymers confined between two flat walls. The film thickness is specified by Δ. The posts with radius R and height H are placed at the substrate of template. L_y and L_z denote the periodicities of post lattice in the y and z directions, respectively. The above system is schematically illustrated in Fig. 1. The melt has n monodisperse AB block copolymer chains, each having a length $N=N_A+N_B$ in terms of the Kuhn length a and gyration radius $R_g=\sqrt{N/6}a$. The volume fraction of A species is denoted as $f_A=N_A/N$. The repulsion between the A and B segments is described by the combined Flory–Huggins interactions $\chi_{AB}N$. The wall profile $\phi_w(\mathbf{x})$ is a smooth function that has a value of one at the walls and decays to zero in the interior of polymeric fluids. The strength of interactions between the I-type segment and wall is specified by the parameter $\chi_{IW}N$ (I = A or B). For simplicity, we assume that the attraction of substrate (s) or air-polymer interface (i) for the preferred segments is equal in magnitude to the repulsion for the non-preferred segments, *i. e.*, $\chi^s_{AW}N=-\chi^s_{BW}N=\chi^sN$ and $-\chi^i_{AW}N=\chi^i_{BW}N=\chi^iN$.

The effective Hamiltonian $\mathscr{H}$ for the system of AB block copolymers in the topographical template has the following form

$$\mathscr{H}\left[W_+,W_-,W^A_{ext},W^B_{ext}\right]/C=\int_V d\mathbf{x}\left[\frac{1}{\chi_{AB}N}W_-^2(\mathbf{x})-\frac{2\zeta N}{\chi_{AB}N+2\zeta N}iW_+(\mathbf{x})-\frac{1}{\chi_{AB}N+2\zeta N}(iW_+(\mathbf{x}))^2+\frac{\chi^iN-\chi^sN}{\chi_{AB}N}\phi_W(\mathbf{x})W_-(\mathbf{x})+\frac{\chi^iN+\chi^sN}{\chi_{AB}N+2\zeta N}\phi_W(\mathbf{x})iW_+(\mathbf{x})\right]-\overline{V}\ln\mathscr{Q}\left[W_+,W_-,W^A_{ext},W^B_{ext}\right] \quad (1)$$

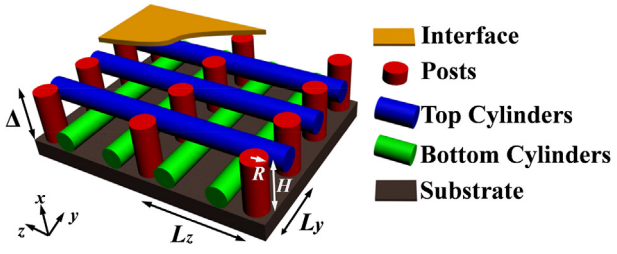

Fig. 1. Schematic representation of directed self-assembly model of block copolymers in topographical template. The block copolymers are confined between the substrate and polymer–air interface and the thickness of topographical template is represented by Δ. The posts with height H and radius R are located at the substrate. The periodicities of post lattice in the y and z directions are specified by L_y and L_z, respectively. The block copolymers in the template equilibrate into 3D structure consisting of two layers of cylinders with perpendicular orientation.

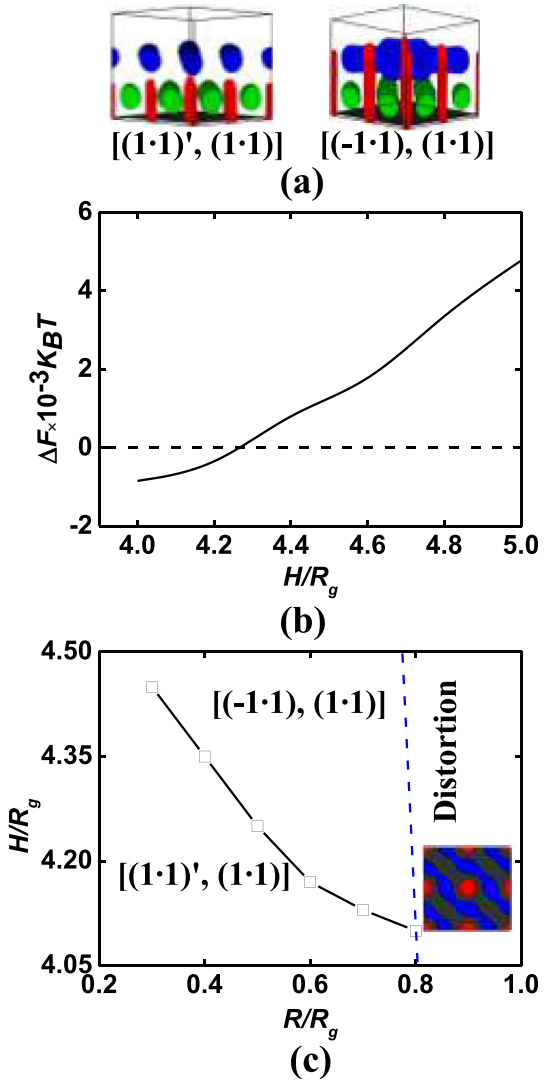

Fig. 2. (a) Candidate structures of block copolymers directed by an array of posts with spacing $L_y = 5.0R_g$ and $L_z = 4.8R_g$. Parallel [(1·1)′, (1·1)] structure at post height $H = 3.0R_g$ and perpendicular [(−1·1), (1·1)] structure at $H = 6.0R_g$. The representations of colors are the same as Fig. 1. (b) Free energy difference $\Delta F \equiv F_{pa}$-F_{pe} between the parallel (pa) and perpendicular (pe) structures as a function of post height H/R_g at fixed post radius $R = 0.5R_g$. The dashed line represents the case of $F_{pa} = F_{pe}$. (c) Relative stability of 3D structures as functions of post height and radius. The phase diagram includes three areas: [(1·1)′, (1·1)], [(−1·1), (1·1)] and distortion structures. The dashed line indicates the approximate boundary of distortion structure. Inset is the top-down view of distortion structure at post radius $R = 0.9R_g$. (For interpretation of the references to colour in this figure legend, the reader is referred to the web version of this article.)

In this expression, $C = \rho_0 R_g^3/N$, $\mathbf{x} = \mathbf{r}/R_g$ and $\overline{V} = V/R_g^3$ are the dimensionless concentration of chains, position and volume, respectively. The stiffness parameter ζN controls the strength of density fluctuations in the Helfand form. W_+ is a pressure field that couples to total density variations, and W_- is an exchange field conjugated to the density difference between the A and B segments. $\mathscr{Q}$ is the normalized single-chain partition function for a diblock copolymer chain. The topographical posts are introduced by additional spatially varying local external fields W_{ext}^A and W_{ext}^B with a hyperbolic tangent form [55,56]. The strength W_0 of external fields is fixed at $W_0 = 40.0$ to prevent the polymers from penetrating into the posts. The steepness ξ_A and ξ_B of the potential change at the well edge for the A and B blocks are set as $0.10R_g$ and $0.20R_g$, respectively. The small value of W_{ext}^A at the well edge promotes the preferential wetting of the A blocks to the posts. While the above field theory of polymeric fluids is formally exact, we restrict our simulations to the mean-field limits named self-consistent field theory, which is given by

$$\left.\frac{\delta\mathscr{H}}{\delta iW_+}\right|_{W_\pm^*} = 0, \quad \left.\frac{\delta\mathscr{H}}{\delta W_-}\right|_{W_\pm^*} = 0 \tag{2}$$

In the present work, the Dirichlet conditions are applied in the x direction, and the periodic boundary conditions are imposed in the y and z directions. The simulation boxes are discretized by using Chebyshev and plane wave basis spectral collocation, which was recently developed by Fredrickson's group [57]. Two types of simulation techniques are applied to fully capture the directed self-assembly behavior of block copolymers in the topographical templates. One is the small cell simulations, which accurately calculate the free energy of 3D ordered structures programmed by the posts. By comparing the free energy of candidate structures, one can identify the stable and metastable configurations of self-assembled block copolymers. The other is the large cell simulations, which help to reduce artifacts and spuriously influence on the observed morphologies. Moreover, the large cell simulations enable us to analyze the orientation behavior of cylinder lines, which cannot be obtained from the small cell calculations. To overcome the computational task, the graphic-processing units using the NVIDIA® CUDA™ architectures are utilized to solve the SCFT equations of polymeric fluids. To reduce the defects of complex structures and increase the correlation length of domain order, a slowly thermal annealing process from a random initial configuration is applied in the large cell simulations. It should be mentioned that a limited number of lattices allocated for each post affects the directed self-assembly behaviors of block copolymers. In our numerical implementation, the self-assembled nanostructures are obtained by considering such limited number of lattices. The different lattice numbers result in the similar 3D structures as long as the spatial resolution of the simulation cells is high enough, *e.g.*, Δy and $\Delta z < 0.20\ R_g$. More details about the model and numerical method could further refer to our previous work [55].

To inspect the local features of 3D ordered structures, another compute program is developed to generate the deformation degree of cylinders. The procedure for the pattern analysis is as follows: The two-dimensional density fields $\langle\phi_A(y,z)\rangle_x^I$ in the y-z plane of I (I = top and bottom) layer are obtained by averaging the density field $\phi_A(x,y,z)$ of minority A blocks along the normal direction of substrate. The fields $\langle\phi_A(y,z)\rangle_x^I$ are then converted into a black-white bitmap. The interfaces between the A- and B-rich domains and the local tangent vectors at the interfaces are derived through the graphical analysis. The angle between the tangent vector and the y axis is specified by θ, which is illustrated in the inset of Fig. 3a. The distributions of angles θ are utilized to characterize the deformation degree of cylinders. The angle θ at the value of higher probability suggests the commensurability orientation of cylinders. As the angle θ is deviated from the commensurability orientation, the cylinders of block copolymers undergo large deformation.

In order to make meaningful predictions for specific systems, it is crucial to establish a connection between the spatial scales of our simulations and the experiments. We achieved this by matching the natural periodicity of block copolymer domains in the bulk with that of simulations using periodic boundary conditions. In our SCFT calculations, the block copolymers are asymmetric with volume fraction $f_A = 0.32$ of A blocks. The chemical incompatibility between the A and B segments is characterized by the combined Flory–Huggins parameter $\chi_{AB}N$, which is set as $\chi_{AB}N = 15.0$ to reflect an effective interaction of system. The block copolymers self-

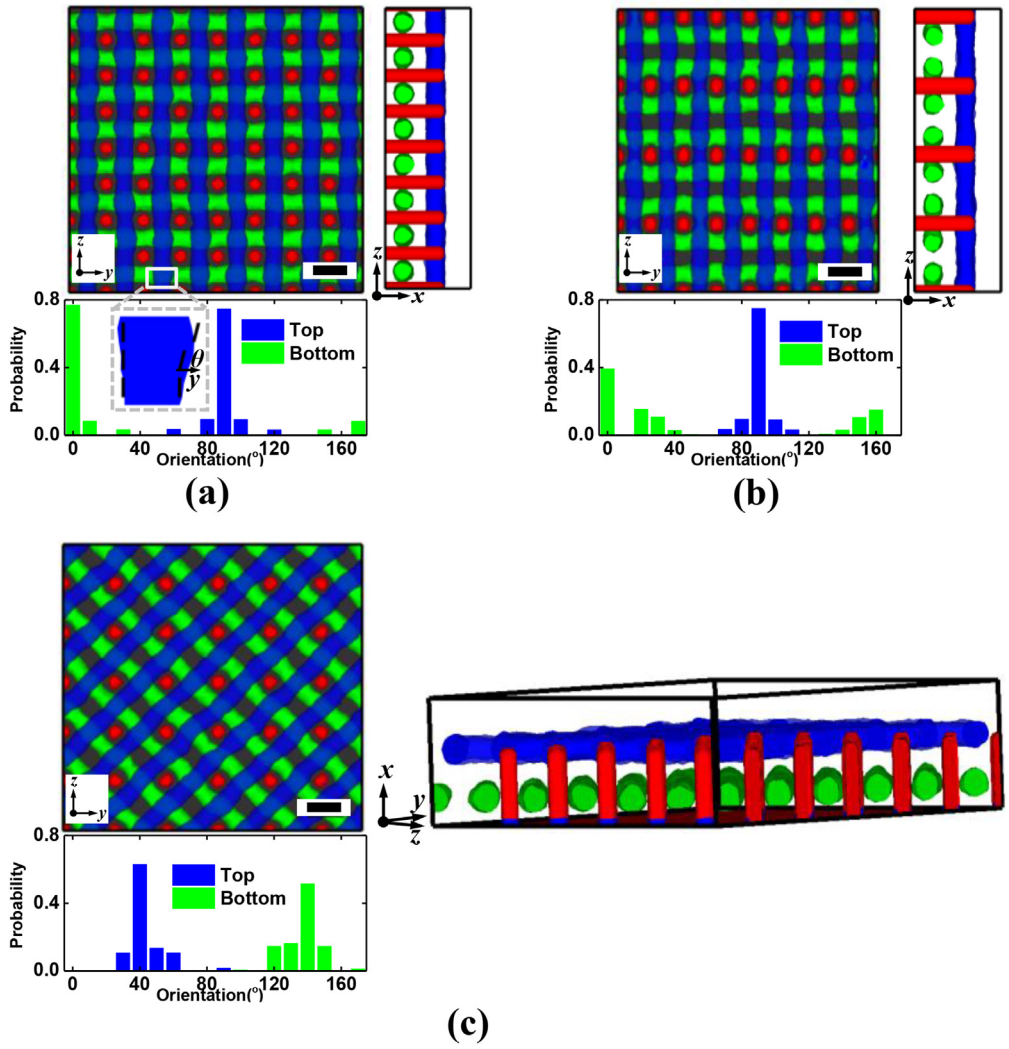

Fig. 3. (Upper panel) Various views and (lower panel) deformation degrees of mesh-shaped structures in topographical templates. (a) [(1·0), (0·1)] structure formed at post spacing $L_y = 3.6R_g$ and $L_z = 3.5R_g$, (b) [(1·0), (0·2)] structure at $L_y = 3.6R_g$ and $L_z = 7.5R_g$, and (c) [(−1·1), (1·1)] structure at $L_y = 5.0R_g$ and $L_z = 4.8R_g$. In the upper panels, the *y*-*z*, *x*-*z* and *x*-*y*-*z* coordinate axes represent the top-down, side and 3D views of ordered structures, respectively. Note that only a portion of patterns are displayed and the polymer–air interfaces are not shown for visualization purpose. Scar bars indicate one natural periodicity of cylinders. The representations of colors are the same as Fig. 1. The deformation degrees of cylinders are characterized by the distribution of angles θ of tangent vectors at the interfaces of cylinders with respect to the *y*-axis, which are schemed in the inset of part (a). (For interpretation of the references to colour in this figure legend, the reader is referred to the web version of this article.)

assemble into the A-rich cylinders with spacing L_0~3.55R_g. Typical experiment samples used in the block copolymer lithography are poly(styrene-*block*-dimethylsiloxane) (PS-*b*-PDMS) with f_{PDMS} = 32.0% and molecular weight of 45.5 kg mol^{-1} [31], which self-assemble into the cylinder structures with natural periodicity ~36 nm. Hence, it is straightforward to estimate the gyration radius of polymer chains in the simulations, *i.e.*, R_g~10 nm, which is used throughout the work to convert the length scales of simulations to the actual sizes. It should be mentioned that the substrates and posts are assumed to be attractive to the majority B blocks and repulsive to the minority A blocks in the simulations of self-assembly of block copolymers directed by the post arrays. But the polymer–air interfaces are attractive to the minority A blocks.

3. Results and discussion

To verify the general feasibility of our simulation approach and to properly evaluate the 3D architectures, we initially performed the large cell simulations of SCFT to probe into the order and orientation behaviors of cylinders in the two-dimensional structures of block copolymer films (Figure S1 of Supplementary Information (SI)). Monolayer of A-rich cylinders with random orientation is formed in the center region of smooth template with thickness $\Delta = 6.0R_g$ (Figure S1a of SI). To impose long-range order on the nanostructures of block copolymers, an array of posts is utilized to register the alignment of cylinders. The in-plane orientation of cylinders is programmed by the periodicities of post lattice (Figures S1b and S1c of SI). As suggested by Ross et al. [58], the single layer of domains is designated as two-dimensional structure.

3.1. Three-dimensional periodic structures

We then carried out the SCFT simulations to systematically investigate the 3D periodic structures of cylindrical-forming block copolymer films. Recently, Li et al. systemically investigated the phase behaviors of block copolymers confined between the smooth substrates [59], and found the transition sequence of structures from the cylindrical monolayers to bilayers as the film thickness

increases. The finding provides useful information for rationally designing the thickness of topographical templates for the 3D programmed nanostructures. In our simulations, multilayers of A-rich cylinders are formed in the center region of topographical templates as the template thickness is set as $\Delta = 9.0R_g$ (Figure S2 of SI). Since the posts with height $H = 3.5R_g$ cannot directly interact with the top cylinders, the orientation of top cylinders is guided by the bottom cylinders instead of the short posts. Such self-registration behavior of block copolymers produces the 3D ordered structures of cylinders with parallel orientation, which limit the specific applications of 3D architectures in the block copolymer lithography.

To independently manipulate the cylinder orientation in each layer, the posts should directly interact with the polymer chains in the upper region of templates. Two important design parameters affecting the interplay between the posts and block copolymers are included in the model of topographical templates: geometrical characteristics (R and H) of posts and periodicities (L_y and L_z) of post lattice. To systematically characterize the 3D structures of block copolymers, we here used the nomenclature $[(a\cdot b), (c\cdot d)]$ as Ross et al. [31], where the two-dimensional Miller indexing (a·b) and (c·d) refer to the top and bottom layers of cylindrical structures, respectively. Specifically, the notation (a·b) is used to index the possible configuration of block copolymer cylinders in the top layers with respect to the post lattices, which satisfies the commensurability conditions $L_0 = (a^2/L_y^2 + b^2/L_z^2)^{-1/2}$. Similarly, the notation (c·d) denotes the cylindrical configuration in the bottom layers. For instance, the 3D structure sketched in Fig. 1 is designated as notation [(1·0), (0·2)]. Here, (1·0) indicates that the top cylinders orient along the z directions, and (0·2) means that the spacing of bottom cylinders is half the periodicity of post lattice in the z direction. As the cylinders place over the posts, a quote is incorporated into the nomenclature. An example is the 3D architecture consisting of the cylinders with parallel orientation as shown in Fig. 2a, which is designated as notation [(1·1)′, (1·1)].

3.1.1. Height and radius of posts

Fig. 2 illustrates control over the cylinder orientation in each layer by changing the geometrical characteristics of posts. To determine the stable configurations, the free energies of various structures are compared. The templates considered here consist of an array of posts with spacing $L_y = 5.0R_g$ and $L_z = 4.8R_g$. Under these settings, the cylinders in the two-dimensional structures are expected to align diagonally with respect to the post lattice, which are demonstrated in Figure S1c of SI. The introduction of the third dimension significantly increases the complexity of self-assembled structures of block copolymer films. Fig. 2a presents the 3D views of two candidate structures. To distinguish the cylinders in different layers, green and blue colors represent the A-rich cylinders in the bottom and top layers, respectively. The posts located at the substrate are denoted as the red color. In the [(1·1)′, (1·1)] structure, the cylinders in both layers orient along the common direction, but the position of top cylinders has a shift. The [(−1·1), (1·1)] structure has two layers of cylinders with perpendicular orientation.

Fig. 2b illustrates the free energy comparison of candidate structures in terms of post height at post radius $R = 0.5R_g$. The free energy difference ΔF is defined as the relative free energy between the competitive structures stated above. The [(1·1)′, (1·1)] structure is stable under the condition of post height $H < 4.3R_g$. The transition of cylinders from the parallel to perpendicular orientations is triggered by the post height. Such phenomenon can be understood as follows: As the parallel structures are programmed by the tall posts, the top A-rich cylinders nearby the B-coated posts are strongly distorted. This results in the enthalpy penalty arising from the increased interface area. To alleviate such effect, the top cylinders are positioned at the gaps of posts. Meanwhile, since the periodicities of posts are diagonally commensurate with the cylindrical dimension, the orientation of cylinders has two possible selections (different diagonal directions of post lattice). To simultaneously reduce the entropy penalty, the cylinders in the top and bottom layers are programmed to orient along different directions. Consequently, the block copolymers are guided to self-assemble into the mesh-shaped structures in the topographical templates with tall posts. It should be mentioned that our extensive SCFT calculations from the random initial configurations reveal that there may exist other possible complicated structures in the block copolymer films, such as the angled mesh-shaped structures, and the 3D structures with the ellipsoids or the perforated lamellae in the bottom layers. To fully discern the stable and metastable phases of the systems, we also compared the free energy of the complicated structures with the candidate structures as shown in Fig. 2a. It is further demonstrated that the cylinders with perpendicular orientation may be the stable phase with the lowest free energy in the case of $H = 6.0R_g$, $L_y = 5.0R_g$ and $L_z = 4.8R_g$.

To evaluate the generality of unique 3D architectures of block copolymer films, we systemically compared the free energy as functions of post height and radius, which allows us to construct stability regions of 3D structures in the two-parameter space, as depicted in Fig. 2c. The phase diagram is divided into three characteristic regions: [(1·1)′, (1·1)], [(−1·1), (1·1)] and distortion structures. As the posts are short, the topographical templates register the orientation of bottom cylinders, which serve as a 'chemical' template to guide the alignment of top cylinders. As a result, the [(1·1)′, (1·1)] structure is stabilized in this region. Increasing the radius and/or height of posts leads to the transition from the [(1·1)′, (1·1)] to [(−1·1), (1·1)] structures. While the radius of posts is large enough, considerable distortion of domains nearby the posts destabilizes the commensurability conditions, implying that the block copolymers cannot self-assemble into long cylinders with controlled orientation. The phenomena result in the distortion structures for the case of the larger posts, as shown in the inset of Fig. 2c. The phase diagram definitely demonstrates that the cylinder orientations in the top and bottom layers are independently manipulated through tuning the geometrical characteristics of posts.

From the application perspectives, the control over the orientation of cylinders in various layers provides a promising approach for fabricating cross-point memory devices via the directed self-assembly of block copolymers [60]. Little has been reported on the formation of such mesh-shaped structures in the experiments and simulations [26,27]. Recent experiments of Ross and coworkers suggested the presence of cylinders with different orientations in the top and bottom layers [31]. However, the morphological details of unique structures are currently difficult to be visualized in the experiments and the 3D ordered architectures in the topographical templates have not been carefully examined in the mesoscale, especially in the large area.

To address these concerns, we here provided detailed insights into the morphologies and the orientation behavior of cylinders in the mesh-shaped structures. For this purpose, the large cell simulations from the completely random initial configurations are performed. To reduce the trap of metastable states of block copolymer films, a gradual annealing process is utilized in the simulations [61]. Fig. 3 illustrates various views of mesh-shaped structures programmed by a rectangular array of posts with height $H = 6.0R_g$. As the periodicities of post lattice are set as $L_y = 3.6R_g$ and $L_z = 3.5R_g$, which are slightly deviated from the commensurability conditions, the orientation of cylinders has two selections, *i.e.*, y and z directions. To alleviate the entropy penalty, the cylinders in each layer are guided to orient along different directions and stack into the

mesh-shaped structure, which is designated as notation [(1·0), (0·1)] (Fig. 3a). Such mesh-shaped structure can be generalized to include holes between the posts. When the periodicity L_z of post lattice is set as $7.5R_g$, double cylinders are accommodated in the gap of posts. As demonstrated in Fig. 3b, the [(1·0), (0·2)] structure is registered by the post array with spacing $L_y = 3.6R_g$ and $L_z = 7.5R_g$, where additional columns of rectangle holes are produced. While the post spacing is set as $L_y = 5.0R_g$ and $L_z = 4.8R_g$, the cylinders are expected to align diagonally with respect to the post lattice (Figure S1c of SI), thereby also having two selections of orientation. As shown in Fig. 3c, the cylinders with different orientations are stacked into the angled mesh-shaped structures.

While the cylinders of block copolymers are perfectly aligned from the top-down views of patterns, the local features of cylinders in the 3D structures remains to be further characterized. To better understand the deformation of domains in various layers, the histograms of angles θ are utilized to characterize the deformation degree of cylinders. Here, θ is defined as the angle between the local tangent vector at the interface of cylinders and y-axis, which is illustrated in the inset of Fig. 3a.

The deformation degrees of cylinders in the top and bottom layers are illustrated in the lower panels of Fig. 3. The histogram represents the probability as a function of the angle grouped into 10° interval. The angles θ with a higher probability correspond to the preferential orientations of cylinders. One can immediately notice that the preferential orientations of cylinders in the bottom and top layers are approximately separated by 90° in the mesh-shaped structures (Fig. 3). However, the cylinders in the parallel structures have the common orientation (Figure S2b of SI). There still exist the angles deviated from the preferential directions due to a small amount of undulations of block copolymer domains nearby the posts or the cross-points of cylinders. Upon close inspection about the distributions, the probability of non-preferential orientations of bottom cylinders is higher than that of top cylinders. The phenomenon manifests the fact that the undulations of cylinders in the top layer are alleviated; namely, the cylinder order in the top layer is enhanced and the top cylinders form the more commensurate arrangement.

3.1.2. Periodicities of post lattice

As stated above, the spacing of posts is a significant factor to register the orientation of cylinders in the topographical templates. Fig. 4 presents the phase diagram of 3D programmed structures in terms of the periodicities of post lattice and summaries the multilayer architectures of self-assembled block copolymers. To construct the phase diagram of 3D ordered structures, the free energy comparisons of candidate architectures are also performed in the small cell simulations. A typical example is illustrated in Figure S3 of SI. In Fig. 4, the periodicities L_y and L_z of post lattice are expressed as the gyration radius R_g of polymer chains or the natural periodicity L_0 of cylinders. The dashed and dotted curves represent the commensurability conditions for the cases of y or z direction and diagonal directions of post lattice, respectively. Due to the symmetry of periodicities L_y and L_z of post lattice, only upper part of the phase diagram is drawn. The parallel and mesh-shaped structures are grouped by the hollow and solid symbols, respectively. The poorly oriented structures are denoted as the small gray dots.

Although the relative stability regions of the registered structures are complicated, there are two notable features in the phase diagram. The first feature is that the top and bottom cylinders sharing the common orientation emerge in the regions of hollow symbols, where only one of the post periodicities is commensurate with the natural periodicity of cylinders. For instance, when the periodicity L_z of post lattice in the z direction is approximately an integral multiple of the natural period L_0 of cylinders while the

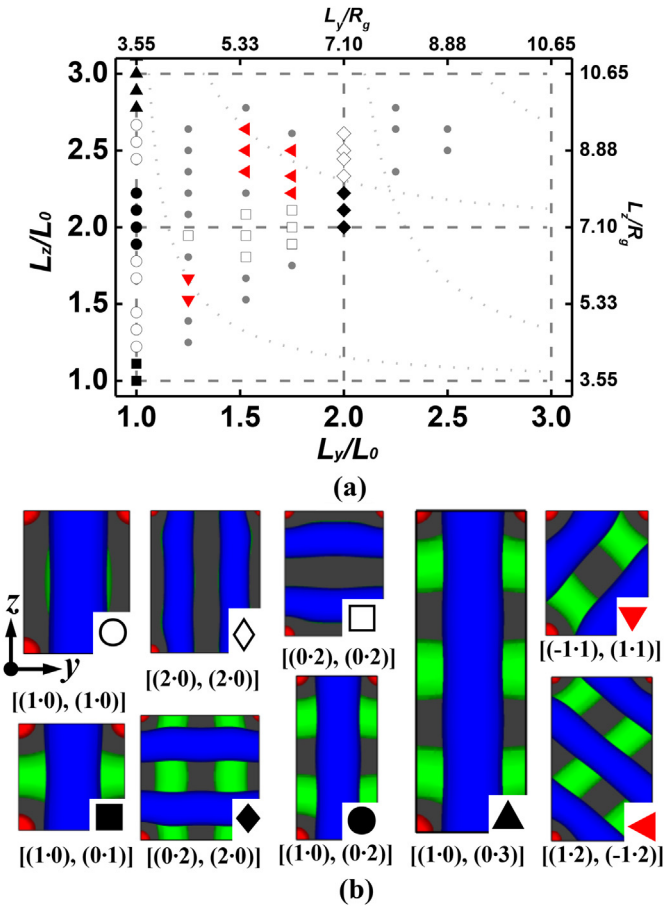

Fig. 4. (a) Summary of 3D ordered structures of cylindrical-forming block copolymers with respect to the periodicities L_y and L_z of post lattice in units of L_0 or R_g. The dashed lines parallel to the horizontal (vertical) axis represent the commensurability conditions for the case of $y(z)$ direction of post lattice. The dotted curves indicate the commensurability conditions for the case of diagonal direction of post lattice. The small gray dots denote the structures of cylinders with poor orientations. (b) Representative 3D structures of block copolymers in topographical templates. The 3D architectures are annotated by the corresponding designations and symbols marked in the phase diagram. The film thickness and post height are set as $\Delta = 9.0R_g$ and $H = 6.0R_g$, respectively.

periodicity L_y is largely deviated from the commensurability conditions, *e.g.*, $L_z \sim 2.0L_0$ and $1.25L_0 \leq L_y \leq 1.75L_0$, the cylinders in both layers are guided to orient along the y direction. As a result, the block copolymers in the topographical templates self-assemble into the [(0·2), (0·2)] structure represented by the hollow squares. Similarly, the [(1·0), (1·0)] and [(2·0), (2·0)] structures are found in the regions satisfied the commensurability conditions only in the y direction.

The second feature is that the mesh-shaped structures appear in the vicinities of the cross-points of dashed lines or the dotted curves. In the former case, where both the periodicities L_y and L_z of post lattice are roughly commensurate with the natural period L_0 of cylinders, two orientations parallel to the y axis and to the z axis are degenerate and equally probable. To reduce the free energy of block copolymer system, the cylinders in various layers are oriented along different directions and stacked into the mesh-shaped structures, *i.e.*, [(1·0), (0·1)], [(1·0), (0·2)], [(1·0), (0·3)], and [(0·2), (2·0)] structures. In the latter case, where the periodicities of posts are diagonally commensurate with the natural periodicity of cylinders, there also exist two possible selections for the cylinder orientation. In the multilayer structures, the cross-cylinder structures with degenerate orientations are formed to alleviate the

entropy penalty. For instance, the cylinders in the top and bottom layers are programmed to orient along the diagonal directions in the [(−1·1), (1·1)] and [(1·2), (−1·2)] structures.

Besides the well-ordered 3D structures, the poorly oriented structures appear in the regions, where the periodicities of post lattice are largely deviated from the commensurability conditions. It should be mentioned that the cylinders in the 3D structures may undergo the morphological transitions as the commensurability conditions are not satisfied. For example, as the template thickness $\Delta = 8.1R_g$ and post periodicities $L_y = 5.0R_g$ and $L_z = 6.0R_g$, the perforated lamellae are embodied in the 3D structures to alleviate the confinement-induced frustration.

The design rules for the 3D ordered structures of cylinder phase, which involve the key factors including the template thickness, the geometrical characteristics of post and the periodicities of post lattice, are also utilized to devise the topographical templates for other self-assembly morphologies of block copolymers. For instance, Figure S4 of SI illustrates the directed self-assembly behavior of spherical-forming block copolymers in the topographical templates. Changing the template thickness leads to a transition from the single layer to double layers of spheres. The post height has a remarkable effect on the position of top spheres and the lattice orientation of sphere arrangement.

3.2. Three-dimensional non-periodic structures

The phase diagrams with respect to the periodicities of post lattice (Fig. 4a) or the height and radius of posts (Fig. 2c), which provide comprehensive pictures over the dependence of 3D periodic structures on the post spacing and geometry, can also provide guidelines to devise the topographical templates for the complex non-periodic structures with specific defects, bend and junctions. In particular, T-junctions are one of the essential geometries of integrated-circuit layouts, but such non-trivial structures at well-defined locations and layers are not achieved in the block copolymer patterns registered by the post arrays with single period.

In light of the design rules for the 3D periodic structures of block copolymers, we theoretically proposed two types of strategies to rationally devise the layouts of post arrays, which are exploited to create the 3D device-oriented superstructures with T-junctions at well-defined locations and desired layers. The first strategy is combination of post arrays with various periodicities in one direction, which satisfy the commensurability conditions of block copolymer cylinders. As depicted in Fig. 5a, the periodicities of post lattices are varied in the z direction, but fixed in the y direction. The combined post arrays direct the block copolymers to self-assemble into the superstructure, where the [(1·0), (1·0)] structure consisting of the parallel cylinders joins with the [(1·0), (0·2)] structure with the perpendicular cylinder arrays. The orientations of top cylinders have a fixed direction while the orientations of bottom cylinders are varied. The T-junctions are located at the well-defined positions of bottom layer, where the cylinders with different orientations meet. Similarly, through integrating the post arrays with various periodicities in the y direction, the mesh-shaped structure meets with the parallel structure (Fig. 5b). In the superstructure, the bottom cylinders have a common orientation while the top cylinders have different orientations. As a result, the T-junctions are formed at the grain boundary of the top layer. It is so far demonstrated that the grain boundaries with 90° angle are generated to form the T-junctions at the desired locations. Satisfying the commensurability conditions and changing the periodicities of post lattice are an effective approach to achieve the T-junctions in the desired layers.

We also noticed that modulating the height of guiding posts has the ability to independently manipulate the orientation of cylinders

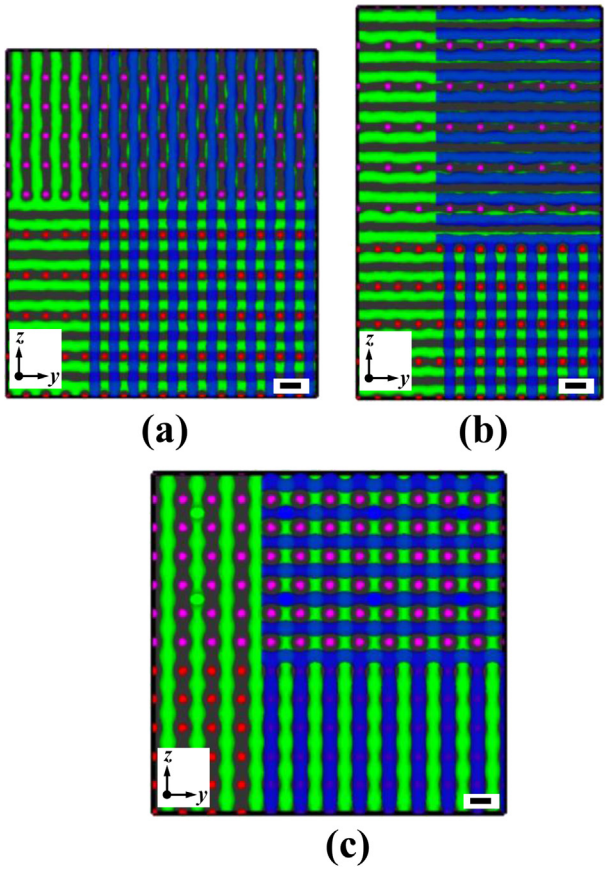

Fig. 5. Three-dimensional non-periodic structures with T-junctions in different layers. (a) Locally controlled pattern by integrating post arrays with different periodicities in the z direction. From the upper part to lower part of image: [(1·0), (1·0)] structure registered by pink posts with spacing $L_y = 3.6R_g$ and $L_z = 5.4R_g$; [(1·0), (0·2)] structure registered by red posts with spacing $L_y = 3.6R_g$ and $L_z = 7.5R_g$. (b) Locally controlled pattern by integrating post arrays with different periodicities in the y direction. [(0·2), (0·2)] structure programmed by pink posts with $L_y = 5.4R_g$ and $L_z = 7.2R_g$; [(1·0), (0·2)] structure programmed by red posts $L_y = 3.6R_g$ and $L_z = 7.2R_g$. (c) Locally controlled pattern by combining post array with various heights. [(0·1), (1·0)] structure registered by pink posts with height $H = 6.0R_g$; [(1·0)′, (1·0)] structure guided by red posts with height $H = 3.0R_g$. Note that a part of top layers are removed for the sake of visualization. (For interpretation of the references to colour in this figure legend, the reader is referred to the web version of this article.)

(Fig. 2), which provides the second route to construct the controlled T-junctions. For example, Fig. 5c shows representative superstructure registered by the arrays of posts with different heights. The complex pattern consists of the parallel structure guided by the short posts and the mesh-shaped structure programmed by the tall posts. The T-junctions are achieved in the top layer due to the orientation change of cylinders. Although both the strategies are able to construct the 3D non-trivial structures, the formed layer and location of T-junctions emerge as a significant difference. The method combining the post spacing makes the T-junctions in the top or bottom layer, depending strongly on the selection of periodicities of post lattice in the y and z directions. Nevertheless, since the post height only affects the orientation of top cylinders, the approach integrating the post height creates the T-junctions only in the top layer. The locations of T-junctions have a shift of half a periodicity due to the self-registration behavior of block copolymers directed by the short posts.

The above simulation results demonstrate that the proposed strategies provide possibilities for precisely constructing the T-junctions through joining the 3D periodic structures with different

orientations of cylinders. Another possible approach regarding this concept is to finely tune the relative positions of cylinder arrays with single orientations. To demonstrate this approach, we devised the layouts of post arrays with a shift of locations in the *z* direction. The effects of relative locations of post arrays on the complex 3D structures are depicted in Figure S5 of SI. The block copolymers are guided to self-assemble into the 3D non-periodic structures with T-junctions in both layers and the superstructures with T-junctions in the bottom layer and jogs in the top layer.

3.3. Three-dimensional interconnected structures

In the 3D architectures illustrated above, the top and bottom cylinders are entirely separated by the matrix, and vertical interconnections between the top and bottom layers are not observed. However, such interconnections play a significant role in enhancing the performance of 3D integrated-circuit systems [40]. Here, we utilized the large cell simulations to examine the influence of template thickness on the interconnection formation in the 3D ordered structures. Fig. 6 shows the structures of block copolymers films in the templates with various thicknesses. The short cylinders perpendicular to the substrate are produced in the template with thickness $\Delta = 7.2R_g$ (Fig. 6a). The cylinder orientation relative to the substrates then changes from perpendicular to parallel as the template thickness increases (Fig. 6b and c). Although the 3D ordered structures are very similar in the top-down views, the local structures below the top layer appear a significant difference from the side view of the patterns. In the case of template thickness $\Delta = 7.8R_g$, the top and bottom cylinders are connected by the A-rich 'necks', which are represented by the green domains in the right panel of Fig. 6b. In the case of template thickness $\Delta = 8.3R_g$, the cylinders in different layers are completely separated by the matrix and the interconnections disappear in the 3D ordered structures.

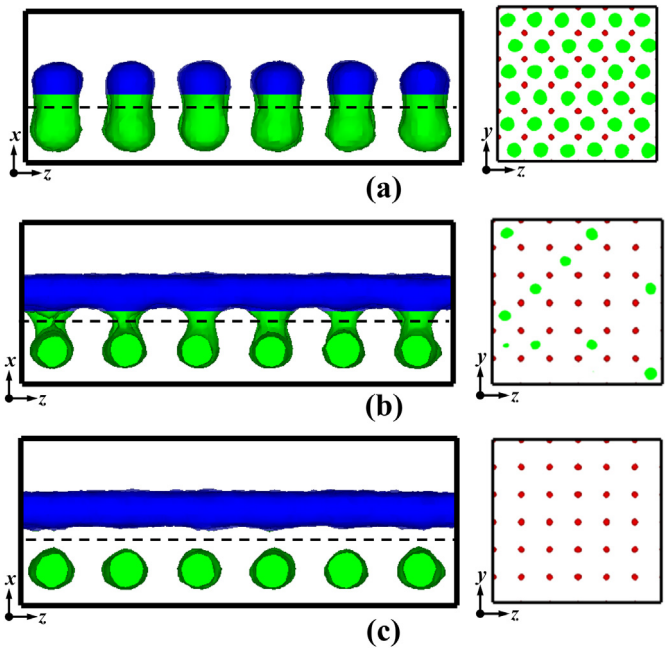

Fig. 6. Effect of template thickness on interconnection between the top and bottom layers. (a) Short cylinders perpendicular to the substrate at template thickness $\Delta = 7.2R_g$, (b) interconnected bilayer structure at $\Delta = 7.8R_g$, and (c) separated bilayer structure at $\Delta = 8.3R_g$. (Left) Side views of self-assembled structures of block copolymers. The posts are not drawn for visualization purpose. (Right) A-block volume fraction distributions in a cross-section at a height marked by the dashed line. The red and green colors represent the posts and A-rich domains, respectively. In the *y*-*z* frame of image (b), the A-rich domains represent the interconnections between the top and bottom layers. (For interpretation of the references to colour in this figure legend, the reader is referred to the web version of this article.)

To quantify the dependence of interconnections on the template thickness, the probability of interconnection formation as a function of template thickness Δ/R_g is plotted in Fig. 7, which is defined as the ratio of the number of interconnections to cross-points of cylinders in the top-down views. Based on how the probability is affected by the template thickness, the curve is divided into three characteristic regions, which are marked by the Roman numbers. In region I, the block copolymers self-assemble into the short cylinders in the center region of templates. Although the probability of interconnections approaches one according to the definition of probability, the block copolymers cannot form the 3D structures under the condition of $\Delta < 7.4R_g$. In region II, the block copolymers self-assemble into the multilayer structures. The interconnections are randomly generated in the mesh-shaped structures. An increase of template thickness alleviates the compression of polymer chains, facilitating the rearrangements of phase-separated domains. The fact results in a decrease of probability of interconnections formed in the 3D ordered structures. Beyond the template thickness $\Delta > 7.9R_g$, the isolated cylinders are unconnected in the multilayer structures.

In Fig. 7, another important outcome is that the interconnections are produced in a very narrow range of template thickness, *e.g.*, $7.4R_g \leq \Delta \leq 7.9R_g$.We could estimate the range of template thickness for the formation of interconnections by plugging in the gyration radius R_g~10 nm, leading to a value of ~5 nm. In addition, the statistical spread in the amount of interconnections increases dramatically as the templates become thick in this range. The above observations suggest that the formation of 3D interconnected structures is strongly dependent on the template thickness, which is a main factor to design the topographical templates for creating the vertical interconnections.

In the recent work of Ross et al. [31], there exist the experimental evidences in the mesh-shaped structures for the vertical interconnections. It is found that the local connections between the top and bottom cylinders are randomly generated in the 3D structures. In the large cell simulations of SCFT, the unique characteristics of 3D interconnected structures are clearly unveiled. Furthermore, the formation range of interconnections in the self-

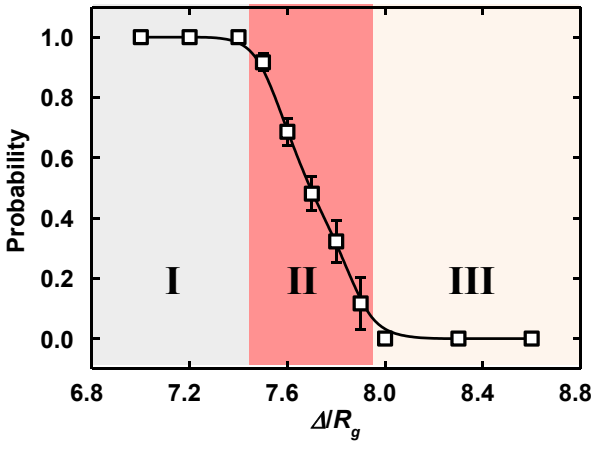

Fig. 7. Probability of interconnection formation as a function of template thickness Δ/R_g. The background colors indicate the different regions marked by Roman numbers. In the regions I-III of template thickness, the block copolymers are guided to self-assemble into the ordered structures depicted in Fig. 6a–c, respectively. Each point is an average of five independent realizations. (For interpretation of the references to colour in this figure legend, the reader is referred to the web version of this article.)

assembled structures is clarified through the simulations. When the thickness of topographical templates is close to the region of transition from the two-dimensional to three-dimensional structures, the block copolymers self-assemble into the coexistence of the connected and unconnected structures due to the small difference of free energy of the configurations, which are observed in Figure S9 of Ref. [31]. However, as the topographical templates become thick, the free energy gap between the connected and unconnected structures is large enough to distinguish the stable structure from a metastable one. As a result, the mesh-shaped structures without the interconnections may survive as the equilibrium morphologies in the large area (Figs. 3 and 6c).

3.4. Discussion

The results of SCFT simulations may have broad implications for explaining the experimental observations and understanding the design rules of 3D periodic and device-oriented patterns in the block copolymer lithography. Almost all the 3D structures of bilayer block copolymer films illustrated in Figs. 3 and 4 can be identified from the existing experimental results. A recent work of Ross and co-workers has reported a variety of 3D structures of cylinders with parallel and angled orientations [31], which are controlled by varying the periodicities of post lattice. As shown in Figs. 3 and 4, the block copolymers are guided to self-assemble into the parallel or mesh-shaped structures. The cylinder orientations in the top and bottom layers are independently manipulated by changing the key design parameters of topographical templates, such as the geometrical characteristics of posts and the periodicities of post lattice (Figs. 2c and 4a). Therefore, the large cell simulations of SCFT capture the morphological characteristics of bilayer block copolymer films and the cylinder orientation behavior of 3D ordered architectures in the experiments.

Beyond reproducing the 3D programmed structures of bilayer block copolymer films, the morphologies obtained from the large cell simulations of SCFT encompass abundant information about the orientation and order behaviors of cylinders in the top and bottom layers. In the experiments, it is currently difficult to capture the interior features of complex patterns through analyzing the images of scanning electron microscope. As depicted in Fig. 3, the various views of mesh-shaped structures clearly demonstrate the cylinder orientations in various layers. From the deformation degrees of cylinders in the top and bottom layers, one can find that the top cylinders form the more commensurate alignment in the mesh-shaped structures, which may help the experimentalists to devise the cross-point memory device in the process of 3D nanofabrication. More recently, Gotrik et al. utilized transmission electron microscope tomography to visualize the morphologies of cylinder bilayers in the topographical templates [35]. It is found that the circularity of top cylinders is larger than that of bottom cylinders. The fact implies that the deformation of top cylinders is small and the block copolymers in the top region of templates self-assemble into the microdomains with more commensurate arrangement, which generally coincide with the predictions of our large cell simulations of SCFT (low panel of Fig. 3).

On the basis of the universal principles of manipulating the 3D periodic structures, we theoretically proposed the strategies to precisely construct the 3D device-oriented elements, such as the T-junctions, the jogs and the interconnections. By joining the 3D architectures of cylinders with various orientations, the controlled T-junctions are formed at well-defined locations and desired layers (Fig. 5). By connecting the 3D architectures of cylinder arrays with a relative shift, the superstructures with the T-junctions and jogs are produced (Figure S5 of SI). The interconnections between the top and bottom layers could be achieved by finely tuning the thickness of topographical templates (Figs. 6 and 7). These results suggest that the rule-based pattern strategies provide a viable approach for constructing the essential geometries of the 3D integrated-circuit layouts. Therefore, it is reasonable to expect that arbitrary structures such as 3D interconnected architectures with controlled jogs and junctions could be patterned using such simple rule-based strategies.

Although the SCFT model presented here provides a powerful tool for studying the directed self-assembly behaviors of block copolymers in the topographical templates, there are still some drawbacks for the case of tackling such complicated systems. Here, a few comments on the model are presented. First of all, due to the complexity of the directed self-assembly of block copolymer films, we only presented the effects of periodicities and geometrical characteristics of posts on the 3D structures for given block copolymer films in the topographical templates (Figs. 2 and 4). The other parameters in the SCFT model, such as the interactions between the A and B blocks, the wetting properties of walls and the selectivity of posts, also have some effects on the directed self-assembly behaviors of block copolymers. For example, a change of the combined Flory–Huggins interaction $\chi_{AB}N$ mainly influences the natural periodicity L_0 of block copolymer microdomains. When the post spacing is commensurate with L_0, the 3D structures of cylindrical-forming block copolymers are very similar to the current case of $\chi_{AB}N = 15.0$. On the other hand, to alleviate the confinement-induced frustration, a morphological transition from the cylinders to perforated lamellae or spheres may take place as the post periodicities are incommensurate with L_0.

Secondly, since there are so many parameters in the SCFT model, the large cell simulations require a substantial amount of computational cost to fully capture the directed self-assembly behaviors of block copolymer films. It is desirable to develop a simple model for predicting the 3D structures in the topographical templates. As a first step along the direction, a theoretical description for the monolayer of cylinders with single orientation has been proposed [62,63]. However, since the 3D structures of block copolymers directed by the posts arrays consist of the multilayer cylinders with different orientations, it is difficult to extend the theoretical framework to comprehensively describe such complex superstructures.

Thirdly, the candidate configurations in the free energy comparison are not the only possible ones due to a large number of periodic and non-periodic structures. We used non-periodic structures with defects as the initial states of small cell simulations, and found that the defective structures with higher free energy density quickly transit into the defect-free structures with lower free energy density as the block copolymers are in the weak segregation region. The behavior coincides with the recent findings of Müller and co-workers [64]. Therefore, the perfect structures of block copolymer films are only considered in the free energy comparison. However, when the interaction parameter $\chi_{AB}N$ increases, the defective structures cannot spontaneously convert into the defect-free states due to the higher free energy barriers. Recent developments in the string method make it possible to identify minimum energy paths between the defective and perfect states [45,65,66]. For example, the string method on the basis of the free energy of SCFT is applied to examine the transition from the dislocation to the defect-free lamellae [45]. This method not only uncovers the mechanism of structure transition, but also provides the free energy barrier for escaping the defective states.

Fourthly, the knowledge of formation process and ordering dynamics of three-dimensional structures is helpful to understand the directed self-assembly mechanism of block copolymers in the topographical templates. The primary difficulty in extending the static to dynamic SCFT is the computational cost due to the

numerical solution of non-linear partial differential equations and the implementation of non-linear conjugate gradient method. To avoid the computational intensity of dynamic SCFT, one can utilize the more coarse-grained model, *e.g.*, the cell dynamics simulations based on the time-dependent Ginzburg-Landau theory. Recently, Li and co-workers applied the method to explore the ordering dynamics of directed self-assembly nanostructures of large-size block copolymer systems [67,68]. It is theoretically demonstrated that the ordering time of block copolymer domains is strongly dependent on the design parameters of templates, which is of great interest for relevant experiments or applications.

4. Conclusions

We performed the large cell simulations to investigate the 3D ordered structures of block copolymer films in the topographical templates. It is demonstrated that increasing the height and radius of posts triggers the transition from the parallel to mesh-shaped structures. The orientations of cylinders in various layers are independently manipulated by varying the periodicities of post lattice. Notably, the deformation degrees of cylinders from the large cell simulations provide the first evidence that the top cylinders form the more commensurate alignment. The combination strategies of post arrays are proposed to precisely construct the 3D non-trivial structures with T-junctions at the well-defined locations and desired layers. Furthermore, it is found that the formation of interconnections between the top and bottom layers is susceptible to the template thickness. Our study enriches the fundamental understanding of the 3D programmed structures of self-assembled block copolymer films, and sheds light on further material design and applications in the 3D nanofabrication.

Acknowledgments

This work was supported by the National Natural Science Foundation of China (51203049, 21234002), Research Fund for the Doctoral Program of Higher Education of China (20120074120003), and the Fundamental Research Funds for the Central Universities.

Appendix A. Supplementary data

Supplementary data related to this article can be found at http://dx.doi.org/10.1016/j.polymer.2015.07.007.

References

[1] G. von Freymann, A. Ledermann, M. Thiel, I. Staude, S. Essig, K. Busch, et al., Three-dimensional nanostructures for photonics, Adv. Func. Mater. 20 (2010) 1038–1052.
[2] C.M. Soukoulis, M. Wegener, Achievements and future challenges in the development of three-dimensional photonic metamaterials, Nat. Phot. 5 (2011) 523–530.
[3] Z.Y. Fan, H. Razavi, J.W. Do, A. Moriwaki, O. Ergen, Y.L. Chueh, et al., Three-dimensional nanopillar-array photovoltaics on low-cost and flexible substrate, Nat. Mater. 8 (2009) 648–653.
[4] Q. Lin, B. Hua, S. Leung, X. Duan, Z. Fan, Efficient light absorption with integrated nanopillar/nanowell arrays for three-dimensional thin-film photovoltaic applications, ACS Nano 7 (2013) 2725–2732.
[5] K. Banerjee, S.J. Souri, P. Kapur, K.C. Saraswat, 3-D ICs: A novel chip design for improving deep-submicrometer interconnect performance and systems-on-chip integration, Proc. IEEE 89 (2001) 602–633.
[6] J.-H. Ahn, H.-S. Kim, K.J. Lee, S. Jeon, S.J. Kang, Y. Sun, et al., Heterogeneous three-dimensional electronics by use of printed semiconductor nanomaterials, Science 314 (2006) 1754–1757.
[7] W. Lu, C.M. Lieber, Nanoelectronics from the bottom up, Nat. Mater. 6 (2007) 841–850.
[8] B.D. Gates, Q. Xu, M. Stewart, D. Ryan, C.G. Willson, G.M. Whitesides, New approaches to nanofabrication: molding, printing, and other techniques, Chem. Rev. 105 (2005) 1171–1196.
[9] S.M. Douglas, H. Dietz, T. Liedl, B. Högberg, F. Graf, W.M. Shih, Self-assembly of DNA into nanoscale three-dimensional shapes, Nature 459 (2009) 414–418.
[10] Y. Ke, L.L. Ong, W.M. Shih, P. Yin, Three-dimensional structures self-assembled from DNA bricks, Science 338 (2012) 1177–1183.
[11] M. Ravnik, G.P. Alexander, J.M. Yeomans, S. Žumer, Three-dimensional colloidal crystals in liquid crystalline blue phases, Proc. Natl. Acad. Sci. U. S. A. 108 (2011) 5188–5192.
[12] F. Rose, J.K. Bosworth, E.A. Dobisz, R. Ruiz, Three-dimensional mesoporous structures fabricated by independent stacking of self-assembled films on suspended membranes, Nanotechnology 22 (2011) 035603.
[13] J.Y. Kim, B.H. Kim, J.O. Hwang, S.-J. Jeong, D.O. Shin, J.H. Mun, et al., Flexible and transferrable self-assembled nanopatterning on chemically modified graphene, Adv. Mater. 25 (2013) 1331–1335.
[14] J.W. Jeong, W.I. Park, L.-M. Do, J.-H. Park, T.-H. Kim, G. Cha, et al., Nanotransfer printing with sub-10 nm resolution realized using directed self-assembly, Adv. Mater. 24 (2012) 3526–3531.
[15] S.O. Kim, B.H. Kim, D. Meng, D.O. Shin, C.M. Koo, H.H. Solak, et al., Novel complex nanostructure from directed assembly of block copolymers on incommensurate surface patterns, Adv. Mater. 19 (2007) 3271–3275.
[16] M.S. Onses, C. Song, L. Williamson, E. Sutanto, P.M. Ferreira, A.G. Alleyne, et al., Hierarchical patterns of three-dimensional block-copolymer films formed by electrohydrodynamic jet printing and self-assembly, Nat. Nanotechnol. 8 (2013) 667–675.
[17] R. Ruiz, E. Dobisz, T.R. Albrecht, Rectangular patterns using block copolymer directed assembly for high bit aspect ratio patterned media, ACS Nano 5 (2011) 79–84.
[18] S.Y. Kim, A. Nunns, J. Gwyther, R.L. Davis, I. Manners, P.M. Chaikin, Large-area nanosquare arrays from shear-aligned block copolymer thin films, Nano Lett. 14 (2014) 5698–5705.
[19] N.A. García, R.L. Davis, S.Y. Kim, P.M. Chaikin, R.A. Register, et al., Mixed-morphology and mixed-orientation block copolymer bilayers, RSC Adv. 4 (2014) 38412–38417.
[20] Z. Zhuang, C. Cai, T. Jian, J. Lin, C. Yang, Self-assembly behavior of rod-coil-rod poly peptide block copolymers, Polymer 55 (2014) 602–610.
[21] X. Yang, Y. Zhu, Y. Wang, Can the individual block in block copolymer be made chromatographically "invisible" at the critical condition of its corresponding homopolymer? Polymer 54 (2013) 3730–3736.
[22] W.-C. Wu, C.-Y. Chen, W.-Y. Lee, W.-C. Chen, Stimuli-responsive conjugated rod-coil block copolymers: synthesis, morphology, and applications, Polymer 65 (2015) A1–A16.
[23] L. Leibler, Theory of microphase separation in block copolymers, Macromolecules 13 (1980) 1602–1617.
[24] T. Ohta, K. Kawasaki, Equilibrium morphology of block copolymer melts, Macromolecules 19 (1986) 2621–2632.
[25] S.X. Ji, U. Nagpal, W. Liao, C.-C. Liu, J.J. de Pablo, P.F. Nealey, Three-dimensional directed assembly of block copolymers together with two-dimensional square and rectangular nanolithography, Adv. Mater. 23 (2011) 3692–3697.
[26] G. Liu, F. Detcheverry, A. Ramírez-Hernández, H. Yoshida, Y. Tada, J.J. de Pablo, et al., Nonbulk complex structures in thin films of symmetric block copolymers on chemically nanopatterned surfaces, Macromolecules 45 (2012) 3986–3992.
[27] A. Ramírez-Hernández, G. Liu, P.F. Nealey, J.J. de Pablo, Symmetric diblock copolymers confined by two nanopatterned surfaces, Macromolecules 45 (2012) 2588–2596.
[28] G. Liu, A. Ramírez-Hernández, H. Yoshida, K. Nygård, D.K. Satapathy, O. Bunk, et al., Morphology of lamellae-forming block copolymer films between two orthogonal chemically nanopatterned striped surfaces, Phys. Rev. Lett. 108 (2012) 065502.
[29] N.L.Y. Wu, X. Zhang, J.N. Murphy, J. Chai, K.D. Harris, J.M. Buriak, Density doubling of block copolymer templated features, Nano Lett. 12 (2011) 264–268.
[30] N.L.Y. Wu, K.D. Harris, J.M. Buriak, Conversion of bilayers of PS-b-PDMS block copolymer into closely packed, aligned silica nanopatterns, ACS Nano 7 (2013) 5595–5606.
[31] K.G.A. Tavakkoli, K.W. Gotrik, A.F. Hannon, A. Alexander-Katz, C.A. Ross, K.K. Berggren, Templating three-dimensional self-assembled structures in bilayer block copolymer films, Science 336 (2012) 1294–1298.
[32] S. Jeon, E. Menard, J.-U. Park, J. Maria, M. Meitl, J. Zaumsei, et al., Three-dimensional nanofabrication with rubber stamps and conformable photomasks, Adv. Mater. 16 (2004) 1369–1373.
[33] L.-R. Bao, X. Cheng, X.D. Huang, L.J. Guo, S.W. Pang, A.F. Yee, Nanoimprinting over topography and multilayer three-dimensional printing, J. Vac. Sci. Technol. B 20 (2002) 2881–2886.
[34] J. Frank, Three-dimensional Electron Microscopy of Macromolecular Assemblies, Oxford University Press, Oxford, 2006.
[35] K.W. Gotrik, T. Lam, A.F. Hannon, W. Bai, Y. Ding, J. Winterstein, et al., 3D TEM tomography of templated bilayer films of block copolymers, Adv. Funct. Mater. 24 (2014) 7689–7697.
[36] M.P. Stoykovich, H. Kang, K.C. Daoulas, G. Liu, C.-C. Liu, J.J. de Pablo, et al., Directed self-assembly of block copolymers for nanolithography: fabrication of isolated features and essential integrated circuit geometries, ACS Nano 1 (2007) 168–175.
[37] G.S. Khaira, J. Qin, G.P. Garner, S. Xiong, L. Wan, R. Ruiz, et al., Evolutionary optimization of directed self-assembly of triblock copolymers on chemically patterned substrates, ACS Macro Lett. 3 (2014) 747–775.

[38] J.-B. Chang, H.K. Choi, A.F. Hannon, A. Alexander-Katz, C.A. Ross, K.K. Berggren, Design rules for self-assembled block copolymer patterns using tiled templates, Nat. Commun. 5 (2014) 3305.
[39] R.S. Patti, Three-dimensional integrated circuits and the future of system-on-chip designs, Proc. IEEE 94 (2006) 1214–1224.
[40] V.F. Pavlidis, E.G. Friedman, Interconnect-based design methodologies for three-dimensional integrated circuits, Proc. IEEE 97 (2009) 123–140.
[41] F.A. Detcheverry, H. Kang, KCh Daoulas, M. Müller, P.F. Nealey, et al., Monte Carlo simulations of a coarse grain model for block copolymers and nanocomposites, Macromolecules 41 (2008) 4989–5001.
[42] F.A. Detcheverry, D.Q. Pike, U. Nagpal, P.F. Nealey, J.J. de Pablo, Theoretically informed coarse grain simulations of block copolymer melts: method and applications, Soft Matter 5 (2009) 4858–4865.
[43] A. Ramírez-Hernández, H.S. Suh, P.F. Nealey, J.J. de Pablo, Symmetric diblock copolymers confined by two nanopatterned surfaces, Macromolecules 47 (2014) 3520–3527.
[44] S.M. Hur, C.J. Garcia-Cervera, E.J. Kramer, G.H. Fredrickson, SCFT simulations of thin film blends of block copolymer and homopolymer laterally confined in a square well, Macromolecules 42 (2009) 5861–5872.
[45] H. Takahashi, N. Laachi, K.T. Delaney, S.-M. Hur, C.J. Weinheimer, D. Shykind, et al., Defectivity in laterally confined lamella-forming diblock dopolymers: thermodynamic and kinetic aspects, Macromolecules 45 (2012) 6253–6265.
[46] B. Kim, N. Laachi, K.T. Delaney, M. Carilli, E.J. Kramer, G.H. Fredrickson, Thermodynamic and kinetic aspects of defectivity in directed self-assembly of cylinder-forming diblock copolymers in laterally confining thin channels, J. Appl. Polym. Sci. 131 (2014) 40790.
[47] W.H. Li, F. Qiu, Y.L. Yang, A.C. Shi, Ordering dynamics of directed self-assembly of block copolymers in periodic two-dimensional fields, Macromolecules 43 (2010) 1644–1650.
[48] X. Man, D. Andelman, H. Orland, Block copolymer at nanopatterned surfaces, Macromolecules 43 (2010) 7261–7268.
[49] P. Chen, H. Liang, R. Xia, J. Qian, X. Feng, Directed self-assembly of block copolymers on sparsely nanopatterned substrates, Macromolecules 46 (2013) 922–926.
[50] Y.A. Kriksin, P.G. Khalatur, I.V. Neratova, A.R. Khokhlov, L.A. Tsarkova, Directed assembly of block copolymers by sparsely patterned substrates, J. Phys. Chem. C 115 (2011) 25185–25200.
[51] M.W. Matsen, In soft matter, in: G. Gompper, M. Schick (Eds.), Polymer Melts and Mixtures, vol. 1, Wiley-VCH, Weinheim, 2006.
[52] G.H. Fredrickson, The Equilibrium Theory of Inhomogeneous Polymers, Oxford University Press, Oxford, 2006.
[53] L. Zhang, J. Lin, Hierarchically ordered nanocomposites self-assembled from linear-alternating block copolymer/nanoparticle mixture, Macromolecules 42 (2009) 1410–1414.
[54] X. Zhu, L. Wang, J. Lin, L. Zhang, Ordered nanostructures self-assembled from block copolymer tethered nanoparticles, ACS Nano 4 (2010) 4979–4988.
[55] L. Zhang, L. Wang, J. Lin, Harnessing anisotropic nanoposts to enhance long-range orientation order of directed self-assembly nanostructures via large cell simulations, ACS Macro Lett. 3 (2014) 712–716.
[56] R.A. Mickiewicz, J.K.W. Yang, A.F. Hannon, Y.-S. Jung, A. Alexander-Katz, K.K. Berggren, et al., Enhancing the potential of block copolymer lithography with polymer self-consistent field theory simulations, Macromolecules 43 (2010) 8290–8295.
[57] S.-M. Hur, C.J. García-Cervera, G.H. Fredrickson, Chebyshev collocation in polymer field theory: application to wetting phenomena, Macromolecules 45 (2012) 2905–2919.
[58] C.A. Ross, K.K. Berggren, J.Y. Cheng, Y.S. Jung, J.-B. Chang, Three-dimensional nanofabri- cation by block copolymer self-assembly, Adv. Mater. 26 (2014) 4386–4396.
[59] W. Li, M. Liu, F. Qiu, A.-C. Shi, Phase diagram of diblock copolymers confined in thin films, J. Chem. Phys. 117 (2013) 5280–5288.
[60] J. Liang, H.S.P. Wong, Cross-point memory array without cell selectors-device characteristics and data storage pattern dependencies, IEEE Trans. Electron Devices 57 (2010) 2531–2538.
[61] S. Hur, A.L. Frischknecht, D.L. Huber, G.H. Fredrickson, Self-consistent field simulations of self- and directed-assembly in a mixed polymer brush, Soft Matter 7 (2011) 8776–8788.
[62] I. Bita, J.K.W. Yang, Y.S. Jung, C.A. Ross, E.L. Thomas, K.K. Berggren, Complex self-assembled patterns using sparse commensurate templates with locally varying motifs, Science 321 (2008) 939–943.
[63] J.K. Yang, Y.S. Jung, J.B. Chang, R.A. Mickiewicz, A. Alexander-Katz, C.A. Ross, et al., Graphoepitaxy of self-assembled block copolymers on two-dimensional periodic patterned templates, Nat. Nanotechnol. 5 (2010) 256–260.
[64] W. Li, P.F. Nealey, J.J. de Pablo, M. Müller, Defect removal in the course of directed self-assembly is facilitated in the vicinity of the order-disorder transition, Phys. Rev. Lett. 113 (2014) 168301.
[65] X. Cheng, L. Lin, E W, P. Zhang, A.-C. Shi, Nucleation of ordered phases in block copolymers, Phys. Rev. Lett. 104 (2010) 148301.
[66] C. Ting, D. Appelö, Z.-G. Wang, Minimum energy path to membrane pore formation and rupture, Phys. Rev. Lett. 106 (2011) 168101.
[67] W. Li, N. Xie, F. Qiu, Y. Yang, A.-C. Shi, Ordering kinetics of block copolymers directed by periodic two-dimensional rectangular fields, J. Chem. Phys. 134 (2011) 144901.
[68] N. Xie, W. Li, F. Qiu, A.-C. Shi, New strategy of nanolithography via controlled block copolymer self-assembly, Soft Matter 9 (2013) 536–542.